A construction of the hat tilings by a Markov partition

Draft, March 26, 2026

Sébastien Labbé* and Peter Selinger†

Abstract

We present a simple construction of hat tilings. The construction can be carried out by superimposing a triangular grid on a specially colored image and reading off the orientation of the tiles. We show that our construction produces valid hat tilings, and conversely, in an appropriate sense that is made precise in the paper, that every valid hat tiling can be obtained in this way.

1 Non-technical overview of the construction

The purpose of this short paper is to present a simple construction of hat tilings [22]. To keep the construction accessible to non-specialists, this introductory section is deliberately written without technical jargon. More mathematical details are given in the later parts of this paper.

The *hat tile* is the following shape. Because it is composed of 8 identical kite-shaped pieces (shown in light gray outlines), it is an example of a shape called a *polykite*.

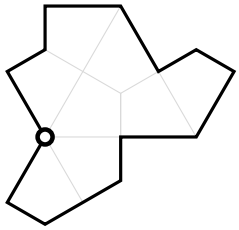

Smith, Myers, and Kaplan [22] discovered that the hat tile has a remarkable property: while it is possible to tile the infinite plane with copies of the hat tile and its mirror image, such tilings can never be periodic. A small section of a hat tiling is shown in Figure 2(a).

Although Smith et al. gave an infinite family of related aperiodic tiles, for simplicity, we focus here on the original "hat" polykite. Our method for constructing a hat tiling is simple. Consider the triangular grid of Figure 3, whose grid points we have marked with small circles. We equip each hat tile with an *anchor* or *control point* that is shown as a small circle above. The tiles will be placed on the triangular grid such that their anchors coincide with grid points. Note that the kites of each hat tile line up with kites on the triangular grid (shown as light gray outlines in Figure 3). Since each hat tile's anchor is incident to four of its kites, forming an angle of $4 \cdot 60° = 240°$, no two distinct tiles can be anchored at the same position. There are 12 possible orientations of the hat tile, which are shown in Figure 1. For convenience, we have colored each tile according to its orientation.

To construct a hat tiling, overlay the triangular grid of Figure 3 on the image of Figure 4. You may shift the grid left, right, up, and down, but you may not rotate it. Place the grid in such a way that none of the grid points fall on the boundaries of the colored regions of Figure 4. Then each grid point lies in a unique

*CNRS – Université de Montréal CRM-CNRS, Montréal, Canada, sebastien.labbe@cnrs.fr
†Dalhousie University, Halifax, Canada, selinger@mathstat.dal.ca

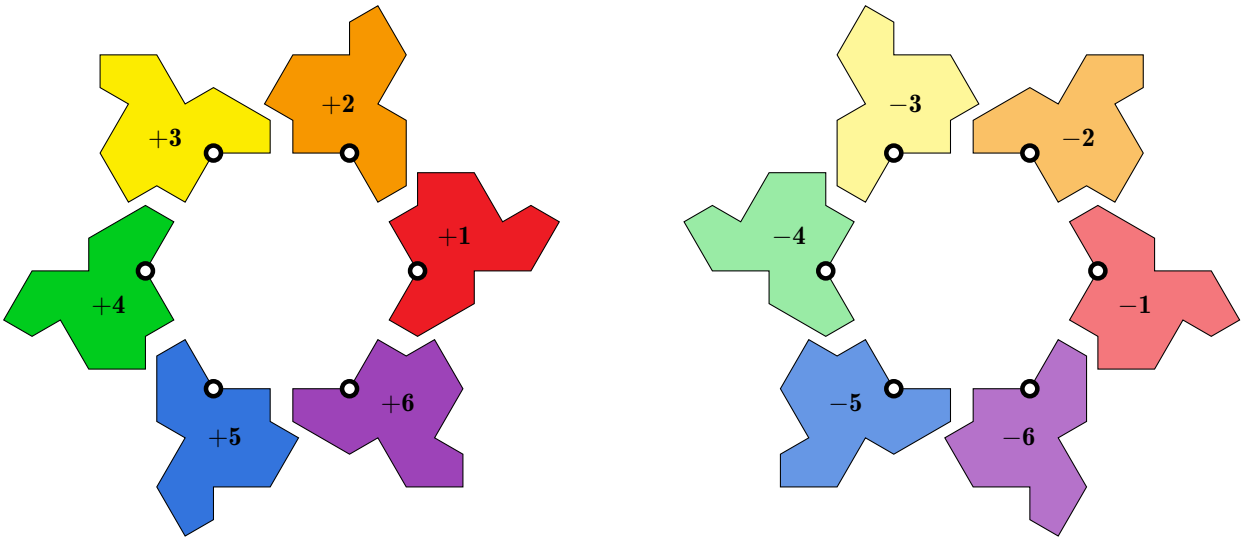

Figure 1: The 12 orientations of the hat tile. To each tile orientation, we assign a unique color and a label in the set $\{+1, +2, +3, +4, +5, +6, -1, -2, -3, -4, -5, -6\}$.

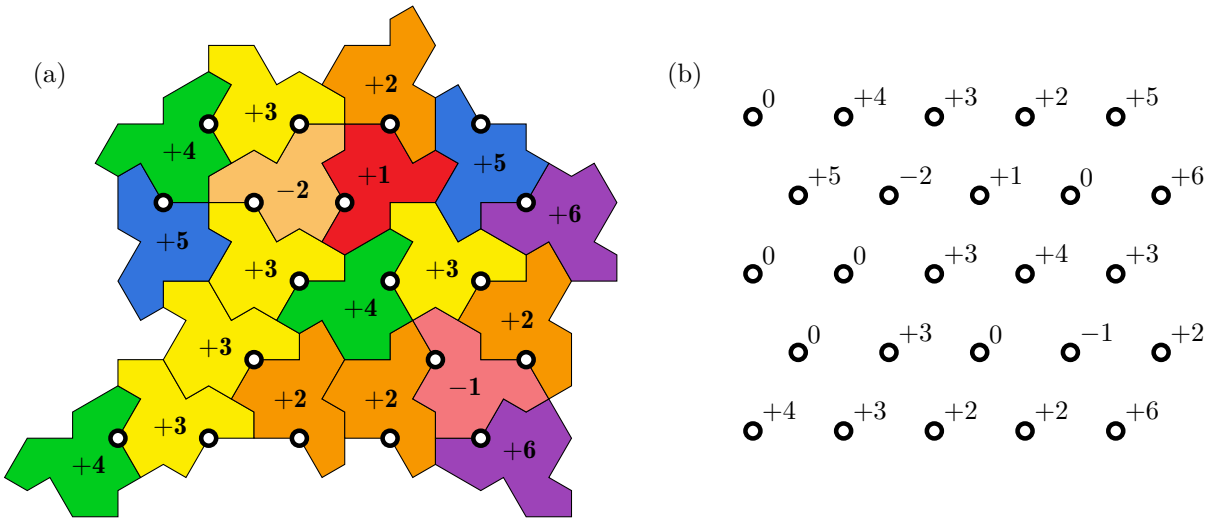

Figure 2: (a) A portion of a hat tiling. The tiles are colored and labelled according to their orientations as in Figure 1. The tiles' anchor points lie on a grid. (b) We have labelled each grid point with the orientation of the tile anchored there, or 0 if no tile is anchored at the point. Note that the tiling is completely determined by the assignment of labels to grid points.

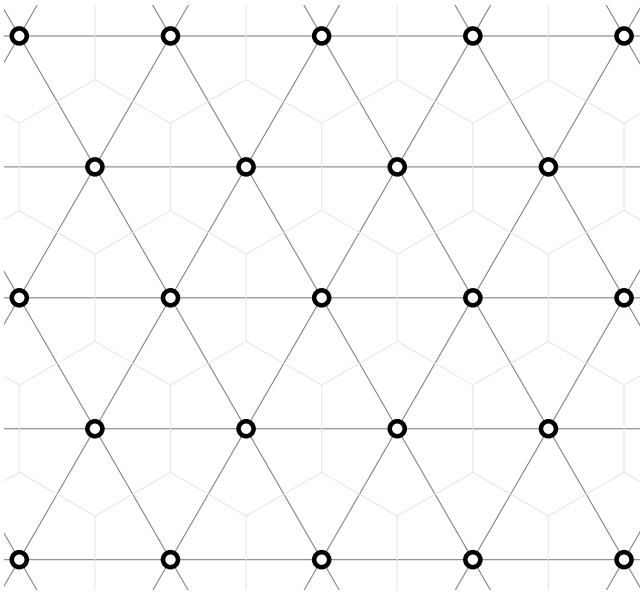

Figure 3: A triangular grid. The grid points are spaced 1 unit apart.

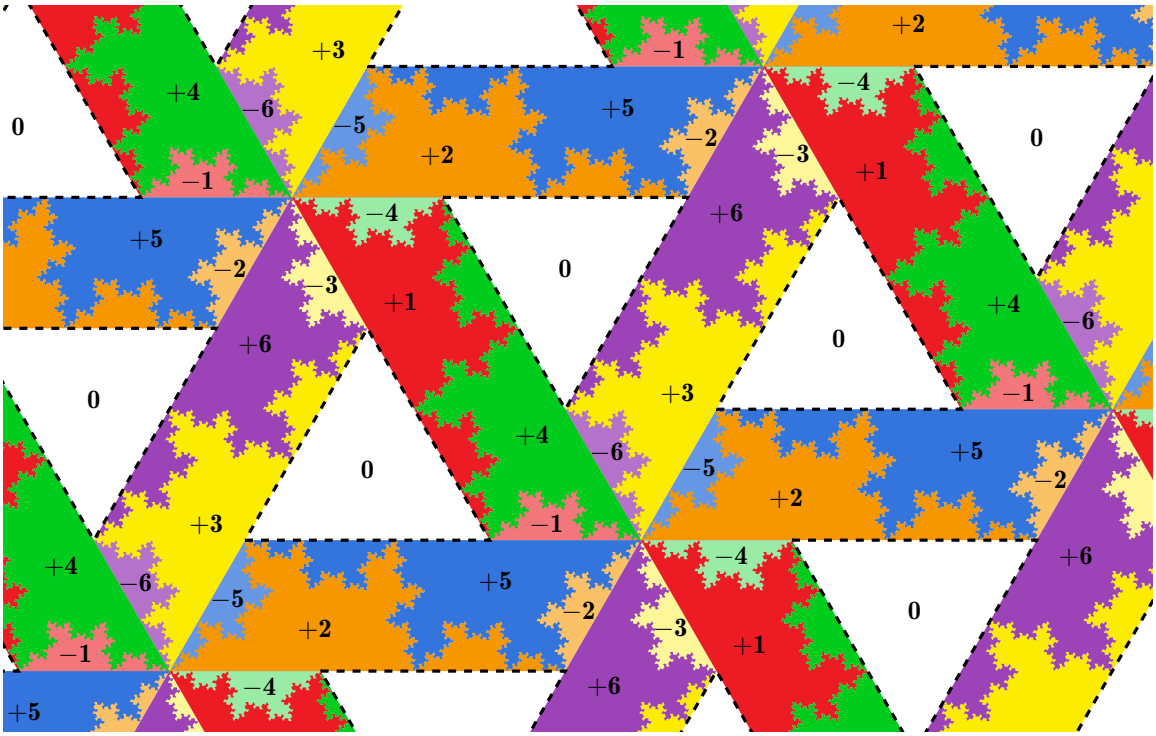

Figure 4: A Markov partition $\mathcal{P}^{+}_{\text{hat}}$ for the hat tiling. We have partitioned the plane into 13 colors: the 12 tile colors, as well as white, indicating the absence of a tile. We use the label 0 for the white regions.

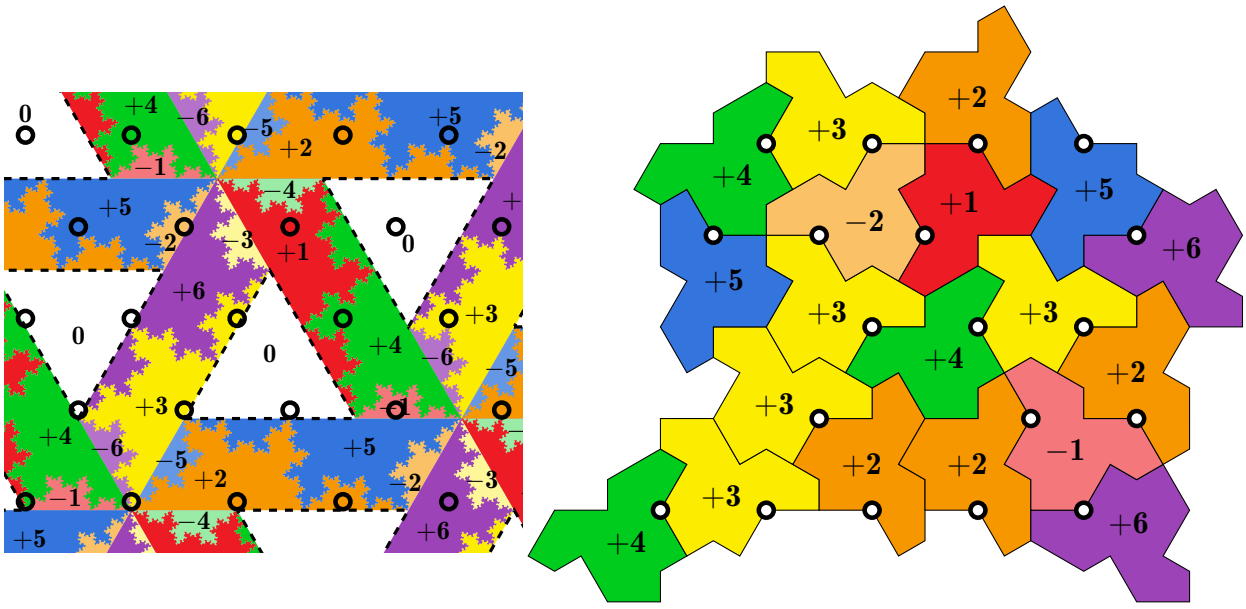

Figure 5: A valid pattern obtained by overlaying the triangular grid on the Markov partition.

colored region. If a grid point's color corresponds to one of the 12 tile orientations, anchor a corresponding tile there. If a grid point lands in a white region, no tile is anchored at it. Figure 5 shows an example of the triangular grid overlaid on the colored image, and the corresponding tiling.

In the remainder of this paper, we explain in more detail how Figure 4 is constructed, and why this construction works.

2 Background and related work

A tiling is a covering of the plane by isometric copies of a set of polygons, called *tiles*, that do not intersect (except on their boundaries). Tilings are often periodic, that is, invariant under a nonzero translation. A set of tiles is called *aperiodic* if it tiles the plane but never periodically. The first aperiodic sets of tiles were discovered more than five centuries ago, as shown by patterns in medieval Islamic architecture [17]. In the West, the first aperiodic sets were discovered by Berger in the 1960's [6, 7] followed by Penrose in the 1970's [18]. The simplest version of Penrose tilings is made of only two tiles. The existence of an aperiodic monotile, i.e., of an aperiodic set made of a single tile, was an open question for 40 years until the recent discovery of the hat tile [22]. The history and theory of aperiodic tilings is vast and will not be further described here. For more information, we refer the reader to these books [9, 4, 21, 5]. For additional work on the hat monotile and its family, see also [1, 23, 3, 2, 19].

Our construction imitates a construction of valid tilings for Jeandel and Rao's aperiodic set of 11 Wang tiles [11]. In [12], the first author showed that valid Jeandel-Rao tilings can be generated by coding the orbit of a $\mathbb{Z}^2$-action by a polygonal partition of the torus. The method of the present paper is the same, but the coding partition is partly fractal and partly polygonal, which makes it unusual and interesting.

Anchors are also sometimes called *control points* [4]. In contrast with [2], where anchor points lie inside or outside of the tiles, our placement of the anchor is on a particular vertex on the boundary of the hat tile.

(a)

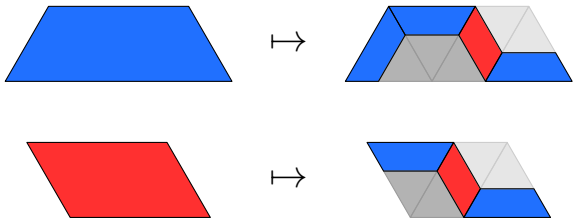

(b)

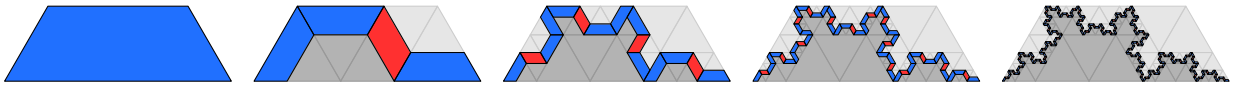

Figure 6: (a) The subdivision rules for the hat fractal. All angles are multiples of 60° and all ratios are golden. (b) The first few subdivision steps.

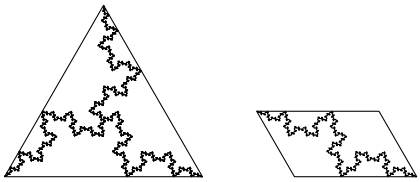

Figure 7: Some symmetries of the hat fractal. The curve generated from the blue segment has a 120° symmetry, and that of the red segment has a 180° symmetry.

3 Our construction, in more detail

3.1 Coordinates

For our purposes, it is convenient to identify the plane with the set of complex numbers. Let $\xi = \exp(\pi i/3)$ be the 6th root of unity. Then every point in the plane can be written as $z = a + b\xi$. The points of the triangular integer grid (Figure 3) are exactly the points with integer coordinates, i.e., points of the form $z = a + b\xi$ where $a, b \in \mathbb{Z}$.

3.2 The hat fractal

The regions of Figure 4 are bounded by straight lines and fractal curves. The fractal is constructed from two types of segments by the recursive decomposition rules shown in Figure 6(a). Some steps of the recursion are shown in Figure 6(b). Note that the fractal decomposition rules are such that the fractal's complement is tiled with triangles of various sizes (shown as gray triangles in Figure 6). With each application of the decomposition rule, the area covered by the blue and red segments decreases by a constant factor. It follows that the fractal curve obtained as the limit of this process has measure 0. Also, as an intersection of infinitely many closed sets, the fractal curve is closed. For each point that doesn't lie on this curve, it is easy to compute which side of the curve is it on, because it will lie in one of the (light or dark) gray triangles.

The hat fractal has several remarkable self-similarities and symmetries. Most relevant for our purposes are the 120° rotational symmetry of the curve obtained from the blue segment and the 180° rotational symmetry of the curve obtained from the red segment (see Figure 7).

The substitution rules defining the hat fractal are very closely related to the "Golden Hex substitution" considered in [1]. The Golden Hex substitution was used to describe a particular member of the hat family

of tilings. Here, we use it to define a partition of the internal space associated with the hat tilings.

Question 3.1. *Describe the relationship between the contracting graph-directed function system defined in Figure 6 and the Golden Hex substitution of [1].*

The hat fractal has been observed before in the description of a partition of the internal space associated with hat tilings [3]. The same fractal shape also appears in [19]. In fact, Figure 8 of [3] and Figure 10 from [2] bear an uncanny resemblance to our Figure 4, although it is not quite the same. More precisely, the number of colors is not the same and, more importantly, the boundaries of the partitions are not the same. Figure 8 from [3] has 4 colors and was obtained by considering the meta-tiles T, H, P and F following the original terminology of [22]. Since these meta-tiles are obtained by a desubstitution process, it is possible that their fractal partition can be obtained as the result of a Rauzy induction on our partition [13] for some hexagonal shape subwindow. For aperiodic tilings by Jeandel-Rao Wang tiles, it was shown [14] that the sequence of 2-dimensional substitutions obtained by a sequence of meta-tiles corresponds to the sequence of substitutions obtained from a Rauzy induction procedure [13] over the partitions of the window of the internal space into polygonal regions. When the partition is made of convex polygons, it is easier to program using convex geometry, but the setup works for non convex (or fractal) regions as well. We leave this question open for now.

Question 3.2. *Describe the relation between our Figure 4 and Figure 8 of [3].*

3.3 Description of the partition

Figure 4 shows a partition $\mathcal{P}^+_{\text{hat}}$ of the infinite plane into 13 colors (the 12 tile colors plus the color white). It is denoted with a plus (+) sign because it describes only tilings where the positively oriented hat is more frequent than the negatively oriented one. The other partition $\mathcal{P}^+_{\text{hat}}$ can be obtained as its mirror image, while also swapping the signs of the labels.

We now describe this partition in more detail. It is obtained by the infinite repetition of a fundamental domain. There are many possible ways of choosing the fundamental domain, and three possibilities are shown in Figure 8. We will first focus on the fundamental domain of Figure 8(c), which is shaped like the recycling symbol ♻. It consists of three parallelograms using complementary colors (red-green, yellow-purple, and blue-orange), as well as two white triangles. The acute angle of each parallelogram is 60°. The sides of the parallelograms have lengths ϕ^2 and 1, respectively, where $\phi = \frac{1+\sqrt{5}}{2}$ is the golden ratio. The white triangles have side length ϕ. Each of the parallelograms is divided into 4 colored regions using segments of the hat fractal, as also shown schematically in Figure 8(c).

We can also consider the parallelogram-shaped fundamental domain shown in Figure 8(a). Its two sides, in complex coordinates, are $v = \phi^2 + \xi$ and $w = \xi(\phi^2 + \xi)$. These two vectors are also the offset vectors by which the fundamental domain repeats (this is irrespective of which presentation of the fundamental domain is chosen). Their linear combinations with integer coefficients generate a lattice, which we denote

$$\Lambda = \langle v, w \rangle_{\mathbb{Z}} = \langle \phi^2 + \xi, \xi(\phi^2 + \xi) \rangle_{\mathbb{Z}} \subset \mathbb{Z}[\phi, \xi] \subset \mathbb{C}.$$

We note that the area of the fundamental domain under translation by this lattice is $\operatorname{Im} v\bar{w} = 2\phi^2\sqrt{3}$, whereas the area of the two white triangles is $\frac{1}{2}\phi^2\sqrt{3}$. Thus, the white triangles make up exactly one quarter of the area of the fundamental region. We also note that the long diagonal of the parallelogram-shaped fundamental domain is $v + w \approx 3.92705 + 3.99933i$. Its vertical offset is very close to 4, but not equal to it. Also, the direction of this diagonal appears at first sight to be 45°, but this is not quite the case.

3.4 Validity of the tiling

We now prove that the partition generates valid tilings. For every generic starting point $x \in \mathbb{C}/\Lambda$ in the torus, the encoding of the shifted lattice $x + \mathbb{Z}[\phi]$ by the partition $\mathcal{P}^+_{\text{hat}}$ defines uniquely a configuration

$$w : x + \mathbb{Z}[\phi] \to \{0, \pm 1, \pm 2, \pm 3, \pm 4, \pm 5, \pm 6\}.$$

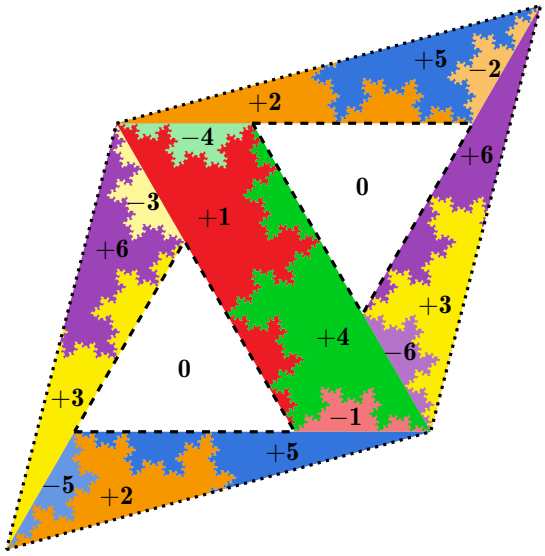

(a) A parallelogram-shaped fundamental domain

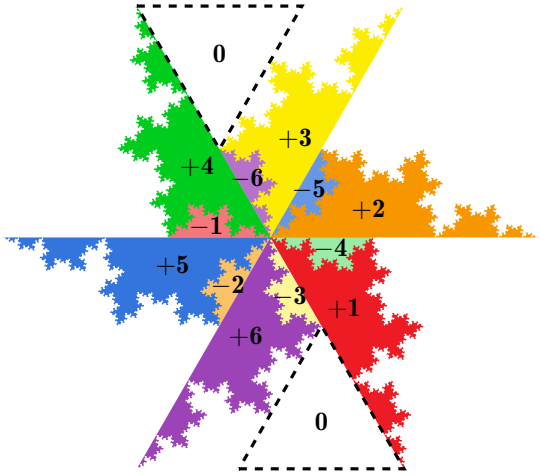

(b) A radially symmetric fundamental domain

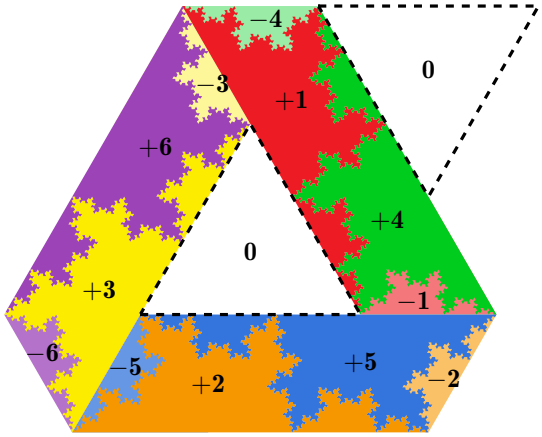

(c) A fundamental domain resembling the recycling symbol ♻. It also resembles the logo of the Canadian Mathematical Society.

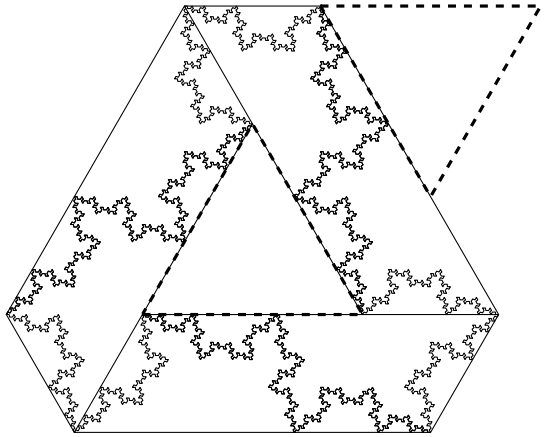

(d) The boundaries of (c)

Figure 8: Partition of the torus $\mathbb{C}/\Lambda$ illustrated on some fundamental domains for the action of Λ on the internal space $\mathbb{C}$. Note that each partition of the fundamental domain includes two white triangles.

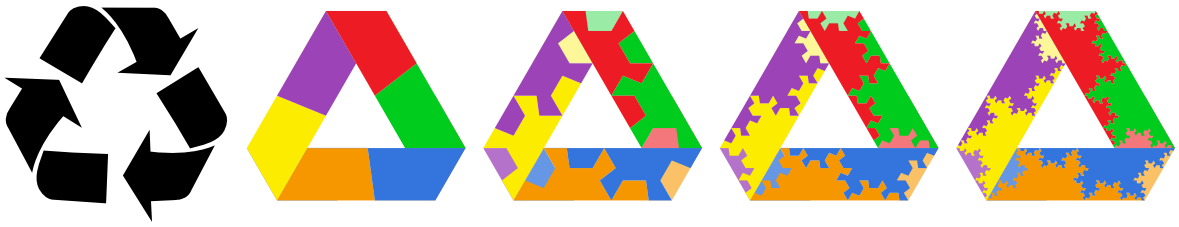

Figure 9: A sequence of partitions converging to the fractal partition $\mathcal{P}^{+}_{\text{hat}}$ of the internal space.

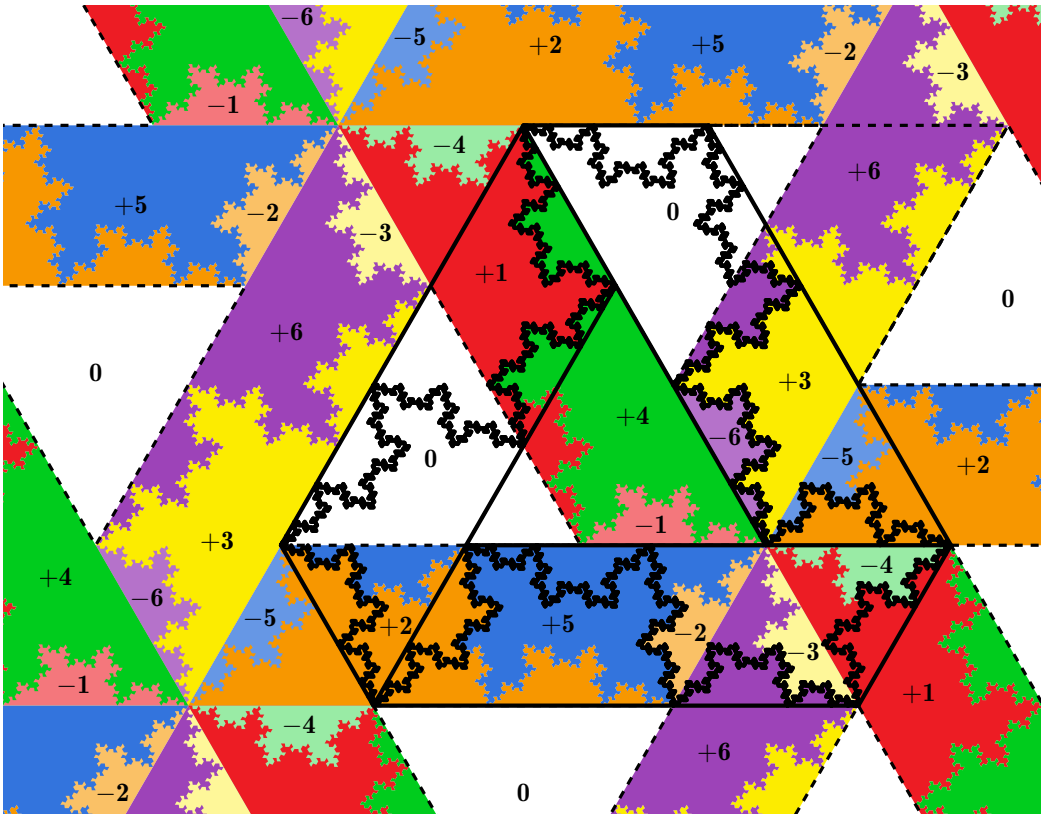

Figure 10: Translating the fundamental region by the vector 1

Proposition 3.3. *For every generic starting point, the configuration generated from the partition describes a valid tiling of the plane by the hat.*

Proof. We must show that no two tiles generated by the partition overlap, and that there are no gaps between the tiles. We first show the no-overlap property. Consider a tile anchored at 0 and another potential tile anchored at 1. We show by case distinction that these tiles do not overlap.

More precisely, from the partition, we deduce, given the tile placed at position $z \in \mathbb{Z}^2$, what are the possible tiles at position $z+1$ in the language of the configurations described by the toral $\mathbb{Z}^2$-action coded by the partition. Specifically, this can be done by inspecting Figure 10, which shows the partition, together with an outline of the fundamental region from Figure 8(d), shifted by 1. For example, the figure shows that the red $+1$ region, shifted by 1, intersects only the regions $+6$, -6, and the white region. The list of intersecting pair of regions is listed in Figure 11. We observe that all pairs of patterns are non-overlapping.

Next, we show the analogous properties for anchors at offset $1+\xi$. Consider a tile A anchored at z and a tile B anchored at $z+1+\xi$. An easy case distinction shows that these tiles only overlap if the orientation of A is in $\{+1,-2\}$ and the orientation of B in $\{+4,-5\}$ (see Figure 12(a)). It is easy to see from Figure 4 that there are no such overlapping pairs: indeed, if we shift the $+1$ region by $1+\xi$, it lies entirely outside of the $+4$ and -5 regions, and similarly if we shift the -2 region.

Next, we must show that there are no overlapping tiles at offset 2. Suppose tile A is anchored at z and tile B is anchored at $z+2$. If they overlap, their respective orientations must either be $+1$ and -4, or -1 and $+4$ (see Figure 12(b)). Again, it is easy to see from Figure 4 that there are no such overlapping pairs: for example, the $+1$ region shifted by an offset of 2 does not overlap the -4 region.

By rotational symmetries, this shows that no two tiles overlap if their anchors are at distance 2 or less. Tiles whose anchors are more than 2 units apart cannot overlap at all; so there are no overlaps in a tiling

Tile at z	Tile at $z+1$	Tile pair pattern
$+1$	$\{+6,-6\}$	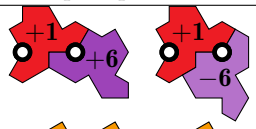
$+2$	$\{+2,+5,+6\}$	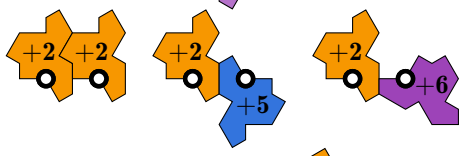
$+3$	$\{+1,+2,+4,+5\}$	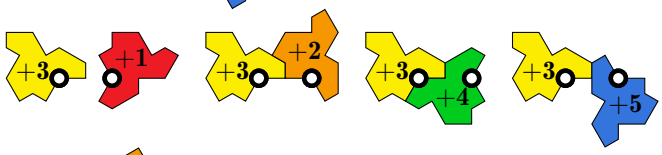
$+4$	$\{+2,+3,+6,-5\}$	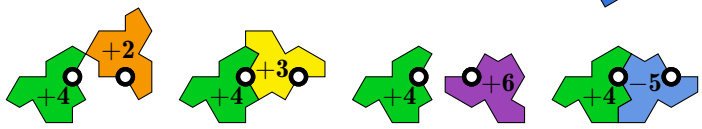
$+5$	$\{+1,+5,+6,$ $-2,-3,-4\}$	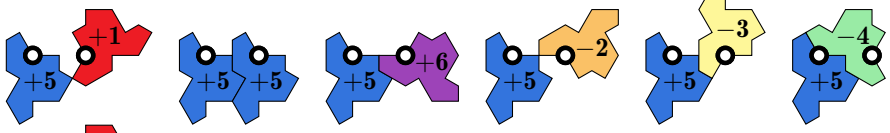
$+6$	$\{+1\}$	

Tile at z	Tile at $z+1$	Tile pair pattern
-1	$\{+2\}$	
-2	$\{+1\}$	
-3	$\{+4\}$	

Tile at z	Tile at $z+1$	Tile pair pattern
-4	$\{0\}$	nothing to check
-5	$\{+2\}$	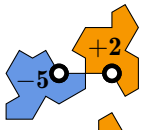
-6	$\{+2\}$	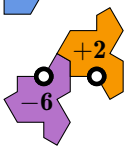

Figure 11: Proof of non-overlap between tiles anchored at z and $z+1$. We do not include anchor points labelled 0, since they have no tile attached to them.

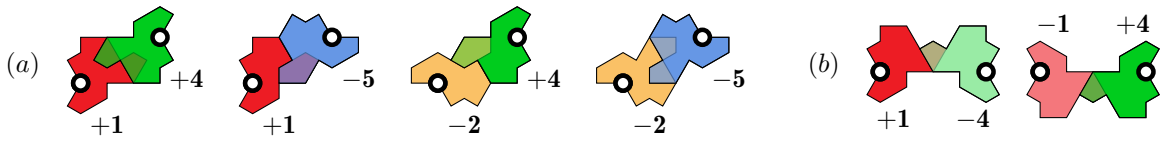

Figure 12: (a) Potential overlap between tiles anchored at 0 and $1+\xi$. (b) Potential overlap between tiles anchored at 0 and 2.

generated by the partition.

To show that there are no gaps between the tiles, assume there was such a gap. Consider the colors of the tiles surrounding the gap (up to some fixed but sufficiently large distance). The colors of these tiles are generated by the corresponding colorings of finitely many points $z_1, \ldots, z_n$ in the partition $\mathcal{P}^+_{\text{hat}}$. Since we assumed the grid to be in general position, none of these points lie on the partition boundaries. Therefore, there exists some $\epsilon > 0$ such that the ϵ-neighborhoods of $z_1, \ldots, z_n$ do not overlap any partition boundaries. This implies that there must be infinitely many places where there is a gap in the tiling, and these places must, in the limit, make up some positive fraction of the anchor points. Then some positive fraction of kites is not covered by a tile.

On the other hand, we noted that the area of the white triangles in the partition is exactly 1/4 of the total area. This means that in our tiling, in the limit, exactly 3/4 of the grid points must anchor a tile. Since each tile covers 8 kites and each anchor point adjoins 6 kites, this implies that each kite is, on average, covered by exactly 1 tile, contradicting the previous paragraph. Hence there are no gaps in the tiling. □

A point on a partition boundary may correspond to more than one valid tiling. A choice can be made as to which set of the partition it belongs to. Other points in its orbit may also fall on the boundary where a consistent choice must be made. The subset of points of an orbit intersecting the partition boundary describes what is a called a *Conway worm*, and the choices of tiles are called its *resolutions* [20]; see also [9, 10.5.8] and [4, Figure 7.22]. Conway worms are usually within bounded distance to a line and can be described by their slope [15]. But, in the context of the hat tilings, it is known that they may have fractal (snake) or linear (Conway worm) shape [23], see also Figure 49 in [24]. Their fractal vs. linear nature can be explained by the fractal and linear nature of the partition's sets, and by the subsets of orbits under the $\mathbb{Z}^2$-action R by horizontal and vertical unit translation on the torus $\mathbb{R}^2/\Lambda$ that remain in its boundary.

4 A Markov partition for the hat tilings

Markov partitions were originally defined for one-dimensional dynamical systems $\mathbb{Z} \overset{R}{\curvearrowright} \mathbb{T}^2$ and were extended to $\mathbb{Z}^d$-actions by automorphisms of compact Abelian groups in [8]. Following [12, 13], we use the notion of Markov partition proposed in [16, §6.5] for dynamical systems defined by a $\mathbb{Z}^2$-action on a torus.

Let M be a compact metric space. Consider $\mathbb{Z}^2 \overset{R}{\curvearrowright} M$, a continuous $\mathbb{Z}^2$-action on M where $R\colon \mathbb{Z}^2 \times M \to M$. For some finite set $\mathcal{A}$, a *topological partition* of M is a collection $\{P_a\}_{a\in\mathcal{A}}$ of disjoint open sets $P_a \subset M$ such that $M = \bigcup_{a\in\mathcal{A}} \overline{P_a}$. If $S \subset \mathbb{Z}^2$ is a finite set, we say that a pattern $w \in \mathcal{A}^S$ is *allowed* for $\mathcal{P}, R$ if

$$\bigcap_{\boldsymbol{k}\in S} R^{-\boldsymbol{k}}(P_{w_{\boldsymbol{k}}}) \neq \varnothing. \tag{1}$$

Let us recall that a $\mathbb{Z}^2$-*subshift* is a set of the form $X \subset \mathcal{A}^{\mathbb{Z}^2}$ which is closed in the prodiscrete topology and invariant under the shift action. Let $\mathcal{L}_{\mathcal{P},R}$ be the collection of all allowed patterns for $\mathcal{P}, R$. The set $\mathcal{L}_{\mathcal{P},R}$ is the language of a subshift $\mathcal{X}_{\mathcal{P},R} \subseteq \mathcal{A}^{\mathbb{Z}^2}$ [10, Prop. 9.2.4]. The subshift $\mathcal{X}_{\mathcal{P},R}$ is called the *symbolic extension* of $\mathbb{Z}^2 \overset{R}{\curvearrowright} M$ determined by the partition $\mathcal{P}$.

For each $x \in \mathcal{X}_{\mathcal{P},R}$ and $m \geqslant 0$, there is a corresponding nonempty open set

$$D_m(x) = \bigcap_{\|\boldsymbol{k}\|_\infty \leqslant m} R^{-\boldsymbol{k}}(P_{x_{\boldsymbol{k}}}) \subset M.$$

The sequence of compact closures $(\overline{D}_m(x))_{m\in\mathbb{N}}$ of these sets is nested and thus it follows that their intersection is nonempty. Notice that there is no reason why $\operatorname{diam}(\overline{D}_m(x))$ should converge to zero, and thus the intersection could contain more than one point. In order for $\mathcal{X}_{\mathcal{P},R}$ to capture the dynamics of $\mathbb{Z}^2 \overset{R}{\curvearrowright} M$, this intersection should contain only one point. This leads to the following definition.

Definition 4.1 ([16])**.** A topological partition $\mathcal{P}$ of M gives a *symbolic representation* $\mathcal{X}_{\mathcal{P},R}$ of $\mathbb{Z}^2 \overset{R}{\curvearrowright} M$ if for every $x \in \mathcal{X}_{\mathcal{P},R}$ the intersection $\bigcap_{m=0}^{\infty} \overline{D}_m(x)$ consists of exactly one point $\rho \in M$. We call x a *symbolic representation of* ρ.

Definition 4.2 ([16, 12, 13])**.** A topological partition $\mathcal{P}$ of $\mathbb{T}^2$ is a *Markov partition* for $\mathbb{Z}^2 \overset{R}{\curvearrowright} \mathbb{T}^2$ if

- $\mathcal{P}$ gives a symbolic representation of $\mathbb{Z}^2 \overset{R}{\curvearrowright} \mathbb{T}^2$ and
- $\mathcal{X}_{\mathcal{P},R}$ is a (2-dimensional) shift of finite type (SFT).

The proof of existence of a Markov partition for Jeandel-Rao tilings was the culmination of a work split into three articles [14, 13, 12]. Here, the proof is simpler because we can use results already known for the hat tilings. The ratio of frequencies of the two orientations of the hat is $[1 : \phi^4]$ or $[\phi^4 : 1]$ [22]. Thus, the set of tilings by the hat splits into two disjoint components

$$\Omega_{\text{hat}} = \Omega^+_{\text{hat}} \cup \Omega^-_{\text{hat}},$$

where Ω^+_{hat} is the component where positive orientations are more frequent. It is known that each component Ω^+_{hat} and Ω^-_{hat} defines a minimal dynamical system for the shift action [22, 3].

On the torus $\mathbb{C}/\Lambda$, we consider the following $\mathbb{Z}^2$-action R acting by horizontal and vertical unit steps:

$$\begin{array}{rccc} R: & \mathbb{Z}^2 \times \mathbb{C}/\Lambda & \to & \mathbb{C}/\Lambda \\ & (\boldsymbol{k}, \boldsymbol{x}) & \mapsto & \boldsymbol{x} + \boldsymbol{k}. \end{array}$$

The $\mathbb{Z}^2$-action R defines a dynamical system $\mathbb{Z}^2 \overset{R}{\curvearrowright} \mathbb{C}/\Lambda$ and we have the following theorem.

Theorem 4.3. *$\mathcal{P}^+_{hat}$ is a Markov partition for the dynamical system $\mathbb{Z}^2 \overset{R}{\curvearrowright} \mathbb{C}/\Lambda$.*

Proof. The fact that the partition $\mathcal{P}^+_{\text{hat}}$ gives a symbolic representation of $\mathbb{Z}^2 \overset{R}{\curvearrowright} \mathbb{C}/\Lambda$ follows from [12, Lemma 3.4] because $\mathbb{Z}^2 \overset{R}{\curvearrowright} \mathbb{C}/\Lambda$ is a minimal dynamical system, and there exists an atom of the partition $\mathcal{P}^+_{\text{hat}}$ which is invariant only under the trivial translation in $\mathbb{C}/\Lambda$.

From Proposition 3.3, the configurations $\mathbb{Z}[\phi] \to \{0, \pm 1, \pm 2, \pm 3, \pm 4, \pm 5, \pm 6\}$ in the set $\mathcal{X}_{\mathcal{P}^+_{\text{hat}},R}$ describe valid tilings. Thus, $\mathcal{X}_{\mathcal{P}^+_{\text{hat}},R} \subseteq \Omega^+_{\text{hat}}$. It is known that Ω^+_{hat} is a minimal dynamical system [22, 3]. We have $\mathcal{X}_{\mathcal{P}^+_{\text{hat}},R} \neq \varnothing$. Therefore, the equality $\mathcal{X}_{\mathcal{P}^+_{\text{hat}},R} = \Omega^+_{\text{hat}}$ holds.

By definition, Ω_{hat} is a shift of finite type. The subset Ω^+_{hat} is also a shift of finite type because it can be described by additional forbidden patterns forcing the hat with negative orientations not to be adjacent. We conclude that the 2-dimensional subshift $\mathcal{X}_{\mathcal{P}^+_{\text{hat}},R}$ is a shift of finite type. Thus, $\mathcal{P}^+_{\text{hat}}$ is a Markov partition for the dynamical system $\mathbb{Z}^2 \overset{R}{\curvearrowright} \mathbb{C}/\Lambda$. □

In lay terms, the above result can be summarized as saying that not only does our Markov partition generate valid hat tilings, but conversely, all valid hat tilings can be generated by our Markov partition (subject to the above provisos about disambiguating points that fall on the partition boundaries, and about generating tilings with more positive than negative hats).

References

[1] S. Akiyama and Y. Araki. An alternative proof for an aperiodic monotile. *Discrete Comput. Geom.*, 74(3):771–792, 2025.

[2] M. Baake, F. Gähler, J. Mazáč, and A. Mitchell. Diffraction of the hat and spectre tilings and some of their relatives. *J. Math. Phys.*, 66(9):092707, 2025. 26 pages.

[3] M. Baake, F. Gähler, and L. Sadun. Dynamics and topology of the hat family of tilings. *Isr. J. Math.*, 270(1):449–485, 2025.

[4] M. Baake and U. Grimm. *Aperiodic Order. Vol. 1*, volume 149 of *Encyclopedia of Mathematics and its Applications*. Cambridge University Press, 2013.

[5] M. Baake and U. Grimm, editors. *Aperiodic order. Volume 2. Crystallography and almost periodicity*, volume 166 of *Encycl. Math. Appl.* Cambridge University Press, 2017.

[6] R. Berger. *The undecidability of the domino problem*. ProQuest LLC, Ann Arbor, Michigan, 1965. Ph.D. Thesis, Harvard University.

[7] R. Berger. The undecidability of the domino problem. *Mem. Amer. Math. Soc. No.*, 66:72, 1966.

[8] M. Einsiedler and K. Schmidt. Markov partitions and homoclinic points of algebraic $\mathbb{Z}^d$-actions. *Tr. Mat. Inst. Steklova*, 216:265–284, 1997.

[9] B. Grünbaum and G. C. Shephard. *Tilings and patterns*. W. H. Freeman and Company, New York, 1987.

[10] M. Hochman. Multidimensional shifts of finite type and sofic shifts. In *Combinatorics, Words and Symbolic Dynamics*, volume 159 of *Encyclopedia Math. Appl.*, pages 296–358. Cambridge University Press, 2016.

[11] E. Jeandel and M. Rao. An aperiodic set of 11 Wang tiles. *Adv. Comb.*, 2021(1), 2021. 37 pages.

[12] S. Labbé. Markov partitions for toral $\mathbb{Z}^2$-rotations featuring Jeandel-Rao Wang shift and model sets. *Ann. H. Lebesgue*, 4:283–324, 2021.

[13] S. Labbé. Rauzy induction of polygon partitions and toral $\mathbb{Z}^2$-rotations. *J. Mod. Dyn.*, 17:481–528, 2021.

[14] S. Labbé. Substitutive structure of Jeandel-Rao aperiodic tilings. *Discrete Comput. Geom.*, 65(3):800–855, 2021.

[15] S. Labbé, C. Mann, and J. McLoud-Mann. Nonexpansive directions in the Jeandel-Rao Wang shift. *Discrete Contin. Dyn. Syst.*, 43(9):3213–3250, 2023.

[16] D. Lind and B. Marcus. *An Introduction to Symbolic Dynamics and Coding*. Cambridge University Press, 1995.

[17] P. J. Lu and P. J. Steinhardt. Decagonal and quasi-crystalline tilings in medieval Islamic architecture. *Science*, 315(5815):1106–1110, Feb. 2007.

[18] R. Penrose. The rôle of aesthetics in pure and applied mathematical research. *Bull. Inst. Math. Appl.*, 10(Jul-Aug):266–271, 1974.

[19] U. Reitebuch. Direct construction of aperiodic tilings with the hat monotile. Available from arXiv:2306.06512, 2023.

[20] E. A. Robinson, Jr. The dynamical properties of Penrose tilings. *Trans. Amer. Math. Soc.*, 348(11):4447–4464, 1996.

[21] M. Senechal. *Quasicrystals and Geometry*. Cambridge University Press, 1995.

[22] D. Smith, J. S. Myers, C. S. Kaplan, and C. Goodman-Strauss. An aperiodic monotile. *Comb. Theory*, 4(1), 2024. Paper No. 6, 91 pages.

[23] J. E. S. Socolar. Quasicrystalline structure of the hat monotile tilings. *Phys. Rev. B*, 108:224109, Dec 2023.

[24] S. Tatham. Finite-state transducers for substitution tilings. Available from arXiv:2512.16595, 2025.